

Multistability of synthetic genetic networks with repressive cell-to-cell communicationEkkehard Ullner,^{1,*} Aneta Koseska,² Jürgen Kurths,^{2,3,4} Evgenii Volkov,⁵ Holger Kantz,⁶ and Jordi García-Ojalvo¹¹*Departament de Física i Enginyeria Nuclear, Universitat Politècnica de Catalunya, Colom 11, E-08222 Terrassa, Spain*²*Center for Dynamics of Complex Systems, University of Potsdam, D-14469 Potsdam, Germany*³*Institute of Physics, Humboldt University Berlin, D-10099 Berlin, Germany*⁴*Potsdam Institute for Climate Impact Research, D-14412 Potsdam, Germany*⁵*Department of Theoretical Physics, Lebedev Physical Institute, Leninskii 53, Moscow, Russia*⁶*Max Planck Institute for the Physics of Complex Systems, Nöthnitzer Strasse 38, D-01187 Dresden, Germany*

(Received 29 April 2008; revised manuscript received 1 July 2008; published 5 September 2008)

We investigate an experimentally feasible synthetic genetic network consisting of two phase repulsively coupled repressilators, which evokes multiple coexisting stable attractors with different features. We perform a bifurcation analysis to determine and classify the dynamical structure of the system. Moreover, some of the dynamical regimes found, such as inhomogeneous steady states and inhomogeneous limit cycles can further be associated with artificial cell differentiation. We also report and characterize the emergence of chaotic dynamics resulting from the intercell coupling.

DOI: [10.1103/PhysRevE.78.031904](https://doi.org/10.1103/PhysRevE.78.031904)

PACS number(s): 87.18.-h, 87.16.Yc, 05.45.-a

I. INTRODUCTION

The design of artificial genetic units resembling submodules of natural circuitry in the cell has led to the construction of bacterial strains that exhibit programmed behavior. Switches [1], oscillators [2,3], and logic gates [4] are well-defined components of artificial genetic networks based on which a complementary approach has been developed, to generate and test hypothetical principles underlying the evolution and operation of biological networks. Most of the artificial components are thus not direct derivatives of natural circuits, but are created to accomplish predefined functions in isolation from the rest of the cellular machinery of the host cell. This approach offers the opportunity to design and study specific functions and signaling pathways for which limitations occur in a natural environment.

Given that cells are frequently subject to chemical signals from neighboring cells, it is a natural step to combine synthetic genetic networks with a chemical cell-to-cell communication mechanism. The ability of cells to communicate with one another allows them to coordinate the behavior of the entire community. A well-defined example of coordinated global behavior in bacteria is, e.g., the quorum sensing mechanism, through which gene expression in bacteria is regulated in response to the local cell population density. In that sense, a recent modeling study has shown the possibility of implementing an enhanced macroscopic genetic clock, consisting of repressilators positively coupled through a quorum-sensing mechanism [5]. That approach enables a diverse and noisy community of synthetic gene oscillators, interacting through a quorum sensing mechanism, to self-synchronize in a robust way, leading to improved rhythmicity of the system. In contrast to such positive coupling, in what follows we consider a cell-to-cell communication module designed to have a repressive and phase-repulsive influence on the repressilator oscillations. It is a

widely accepted fact that a phase repulsive coupling [6–8] leads to competition and avoidance between network components in physics and biology, and is used, e.g., to explain morphogenesis in Hydra regeneration and animal coat pattern formation [9], neural activity in the brain of songbirds [10], regulation in the respiratory system [11], and global behavior of synthetic genetic networks [12,13].

Recently, we showed that a repressilator population consisting of 100 cells with repressive cell-to-cell communication offers a very diverse dynamics, due to the inherited multistability and multirhythmicity [13], and exhibits a high adaptability typical of natural systems. These effects can be very important for the construction of genetic networks and understanding of evolutionary effects behind the mechanisms of cell differentiation and genetic clocks. The ability of a genetic unit to produce different dynamical regimes that coexist provides improved adaptability: If a cellular state becomes unprofitable for the cell, the genetic unit can easily switch to some of the other available coexistent states. Therefore, in the present paper we perform a detailed bifurcation analysis of a minimal system of two repressilators coupled via repressive cell-to-cell communication, in a biologically realistic parameter range. The analysis reveals the dynamical structure of the model, allowing us to classify the character of the regimes present and explaining in detail the transitions between them. Moreover, we report and discuss in detail a chaotic regime found in certain parameter ranges. It is important to note here that the discussed repressilator is, to our knowledge, the first synthetic genetic model displaying chaotic dynamics in a biologically reasonable parameter range. We further discuss the importance of these dynamical regimes in coupled genetic networks for new applications regarding the design of genetic clocks, synchronization properties with the cell cycle [14], chronotherapy, etc.

II. MODIFIED REPRESSILATOR WITH REPRESSIVE CELL-TO-CELL COMMUNICATION

The repressilator consists of three genes whose protein products repress the transcriptions of each other in a cyclic

*ekkehard.ullner@upc.edu

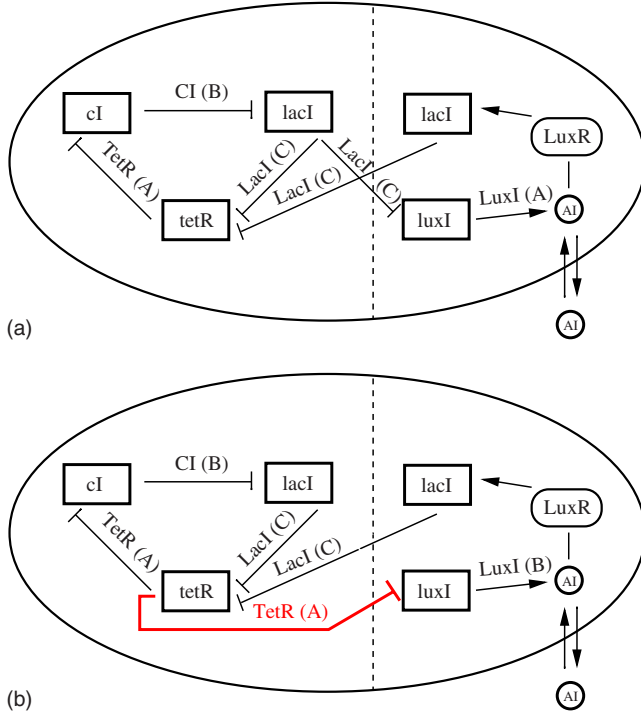


FIG. 1. (Color online) Scheme of the repressilator with quorum sensing cell-to-cell communication: with reinforcing coupling [5] (top) and repressive coupling (bottom).

way [2]. The gene *lacI* expresses protein LacI, which inhibits transcription of the gene *tetR*. The product of the latter, TetR, inhibits transcription of the gene *cI*. Finally, the protein product CI of the gene *cI* inhibits expression of *lacI* and completes the cycle (left-hand module in Fig. 1). An additional feedback loop involving two proteins, LuxI and LuxR, placed on a separate plasmid, realizes the cell-to-cell communication [5,15,16]. The LuxI protein is responsible for the biosynthesis of a specific, acylated homoserine lactone signaling molecule, known as the autoinducer (AI). The autoinducer is a small molecule that can diffuse through the cell membrane, providing the means for chemical communication between neighboring cells. It binds the LuxR protein, and the LuxR-AI complex further activates targeted gene expression, in this case, the additional *lacI* gene.

In [5] it was suggested to place the gene *luxI* under inhibitory control of the repressor protein LacI (Fig. 1 top). The additional negative feedback loop in this case coincides with the overall negative feedback along the repressilator ring and evokes a reinforced coupling. An ensemble of repressilators engineered in this way tends to achieve in-phase oscillations with strong global self-oscillations. However, in contrast to [5] we investigate here the case of a repressive and phase-repulsive coupling. For this purpose, we have modified the initial scheme (top module in Fig. 1), placing the gene *luxI* under inhibitory control of the repressilator protein TetR (Fig. 1 bottom). The proposed rewiring between the repressilator and the quorum sensing module introduces an additional loop which competes with the overall negative feedback loop along the repressilator ring, resulting in a phase-repulsive intercellular coupling.

The mRNA dynamics is described by the following Hill-type kinetics with Hill coefficient n :

$$\dot{a}_i = -a_i + \frac{\alpha}{1 + C_i^n}, \quad (1)$$

$$\dot{b}_i = -b_i + \frac{\alpha}{1 + A_i^n}, \quad (2)$$

$$\dot{c}_i = -c_i + \frac{\alpha}{1 + B_i^n} + \kappa \frac{S_i}{1 + S_i}, \quad (3)$$

where the subindex i specifies the cell, and a_i , b_i , and c_i represent the concentrations of mRNA molecules transcribed from the genes of *tetR*, *cI*, and *lacI*, respectively. The model is made dimensionless by measuring time in units of the mRNA lifetime (assumed equal for all genes) and the mRNA and protein levels in units of their Michaelis constants. The mRNA concentrations are additionally rescaled by the ratio of their protein degradation and translation rates. α is the dimensionless transcription rate in the absence of a repressor (assumed equal). κ is the maximum transcription rate of the LuxR promoter. The dynamics of the proteins is linked to the amount of the responsible mRNA, and the parameter $\beta_{a,b,c}$ describes the ratio between mRNA and the protein lifetimes (inverse degradation rates). We assume different lifetime ratios for the protein-mRNA pairs which results in a weak relaxatorlike dynamic of the repressilator.

The variables A_i , B_i , and C_i denote the concentration of the proteins TetR, CI, and LacI, which have dynamics given by

$$\dot{A}_i = \beta_a(a_i - A_i), \quad (4)$$

$$\dot{B}_i = \beta_b(b_i - B_i), \quad (5)$$

$$\dot{C}_i = \beta_c(c_i - C_i). \quad (6)$$

The cell-to-cell communication is realized by the small autoinducer protein (AI). Assuming equal lifetime of the CI and LuxI proteins, their dynamics are identical, and hence we will use the same variable to describe both protein concentrations. The AI concentration S_i in cell i is proportional to B_i , i.e., the concentration of LuxI protein in it. The AI concentration S_i is scaled by its Michaelis constant as well. The dynamics of the internal AI is also affected by an intracellular degradation, and by diffusion toward or from the intercellular space,

$$\dot{S}_i = -k_{s0}S_i + k_{s1}B_i - \eta(S_i - S_e), \quad (7)$$

$$S_e = Q\bar{S}, \quad (8)$$

$$\bar{S} = \frac{1}{N} \sum_{i=1}^N S_i. \quad (9)$$

The diffusion coefficient η depends on the permeability of the membrane to the autoinducer. Due to the fast diffusion of

the extra-cellular AI (S_e) compared to the repressilator period, we can apply the quasi-steady-state approximation to the dynamics of the external AI and replace the dynamics of the extra-cellular AI S_e by the mean field of the internal AI \bar{S} [5].

The parameter Q is defined as $Q = \delta N / V_{\text{ext}} / k_{se} + \delta N / V_{\text{ext}}$ [5], with N the number of cells, V_{ext} the total extra-cellular volume, k_{se} the extra-cellular AI degradation rate, and δ the product of the membrane permeability and the surface area. The coupling coefficient Q is proportional to the cell density and can be varied in the range between 0 and 1 in a controlled way in a chemostat experiment by changing the total chemostat volume. Therefore, in the numerical investigations that follow we use Q as bifurcation parameter.

The parameter values used, given in the caption of Fig. 2, are experimentally reasonable, corresponding to mRNA lifetimes of 5 min, a TetR protein lifetime of 5.9 min, a CI and LacI protein lifetime of 50 min, an AI lifetime of 5 min, Michaelis constants of 20 nM, translation rates of 0.1 proteins/s, and an unrepressed transcription rate of 0.4 transcripts/s for *tetR* and 0.047 transcripts/s for *cI* and *lacI*. We assume $k_{se} \sim 0.6 \text{ h}^{-1}$, which is reasonable for a medium with $\text{pH} \sim 7$ [16]. The membrane permeability coefficient for the AI corresponds to 10^{-9} m/s , which is on the order of magnitude of similarly sized biomolecules, such as tryptophan and glucose [17].

III. BIFURCATION ANALYSIS FOR TWO COUPLED REPRESSILATORS

Models of synthetic genetic applets usually either consist of single synthetic units [1,2] or exhibit in-phase oscillatory behavior [3,5]. On the other hand, other regimes including clustering, with the possibility of different distributions between clusters, have been reported recently in networks of synthetic genetic oscillators of different types [12,13]. In particular, the model described in the preceding section exhibits multistability and oscillation death [13]. Figure 2 shows representative time traces, obtained by direct numerical calculations of a population of $N=2$ coupled repressilators, for increasing coupling strength. The different dynamical regimes found are self-sustained oscillatory solutions [Fig. 2(a)], inhomogeneous limit cycles (IHLC) [Fig. 2(b)], inhomogeneous steady states (IHSS) [Fig. 2(c)], and homogeneous steady states (HSS) [Fig. 2(d)], all of which exist for biologically realistic parameter ranges. Here we present a detailed bifurcation analysis that allows us to determine the origin of the different solutions and the scenarios of transitions between them, thus providing deeper qualitative and quantitative conclusions about the structure and dynamical behavior of the system.

The analysis is performed using the XPPAUT package [18] for a system of two coupled genetic oscillators, and shows that already two oscillators provide a large variety of possible regimes. In the bifurcation analysis below we use the coupling strength Q [Eq. (8)] as a biologically relevant parameter to obtain one-parameter continuation diagrams. Q is proportional to the cell density and can be changed experimentally in chemostat experiments in the range between zero

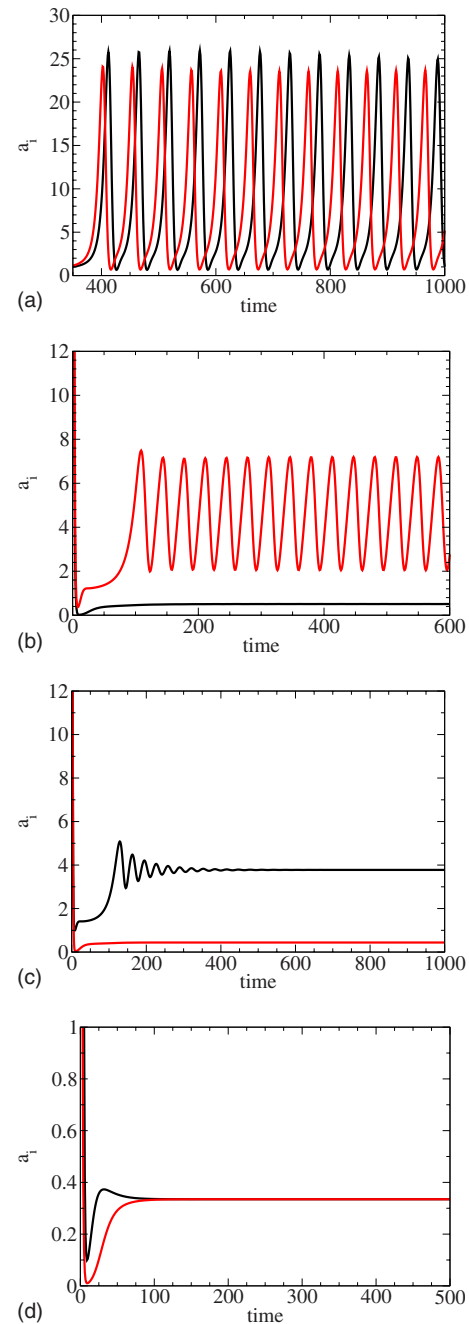


FIG. 2. (Color online) Typical time series of the a_i mRNA concentration for the four stable regimes: (a) $Q=0.1$, oscillatory; (b) $Q=0.3$, inhomogeneous limit cycle; (c) $Q=0.4$, inhomogeneous steady state; and (d) $Q=0.4$, homogeneous steady state. The common parameters are $N=2$, $n=2.6$, $\alpha=216$, $\beta_a=0.85$, $\beta_b=0.1$, $\beta_c=0.1$, $\kappa=25$, $k_{s0}=1.0$, $k_{s1}=0.01$, $\eta=2.0$.

and one. Values beyond this range do not have biological meaning, but can be helpful for a formal bifurcation analysis. Thus, starting from the homogeneous unstable steady state of isolated oscillators ($Q=0$), we have obtained the basic continuation curve containing the homogeneous and inhomogeneous stable steady states (the stability regions of HSS and IHSS are shown on Fig. 3). It is necessary to mention here that the bifurcation diagrams shown in what follows (Figs.

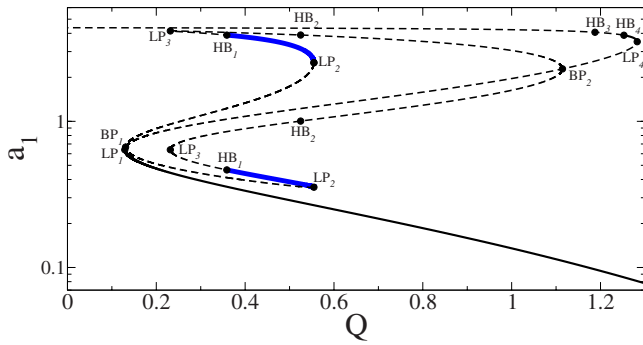


FIG. 3. (Color online) Bifurcation diagram obtained by variation of Q , illustrating the stable-steady-state regimes (HSS and IHSS). For parameters values see Fig. 2. Here, thin solid lines denote the HSS, thick solid lines the IHSS, and dashed lines denote unstable steady states. The same bifurcation diagram is valid for the second repressilator.

3–5) depict only those bifurcation points and solutions that are in the center of the corresponding discussion.

The basic continuation curve is characterized by two important properties: (1) the presence of broken symmetry bifurcations (BP_1 and BP_2 in Fig. 3) where inhomogeneous solutions arise, and (2) the stabilization of the homogeneous state for large coupling values ($Q > 0.129$). The HSS solution is characterized by a constant protein level concentration, stabilized through a saddle node bifurcation (LP_1 in Fig. 3). A typical time series of this regime can be seen in Fig. 2(d). Additionally, another HSS branch is found between LP_4 and HB_4 (Fig. 3), but it is located outside the biological relevant range (since $Q > 1$).

As a result of the symmetry breaking of the system through a pitchfork bifurcation (BP_1 in Fig. 3), the unstable steady state splits in two additional branches, giving rise to an inhomogeneous steady state (IHSS). This particular phenomenon is model-independent, persisting for large parametric regions in several models of diffusively coupled chemical [19–21] or biological oscillators [3,22]. The IHSS in our model is manifested through two distinct steady protein concentration levels [Fig. 2(c)], gaining stability through a Hopf bifurcation, denoted as HB_1 in Fig. 3, and thus leading to the

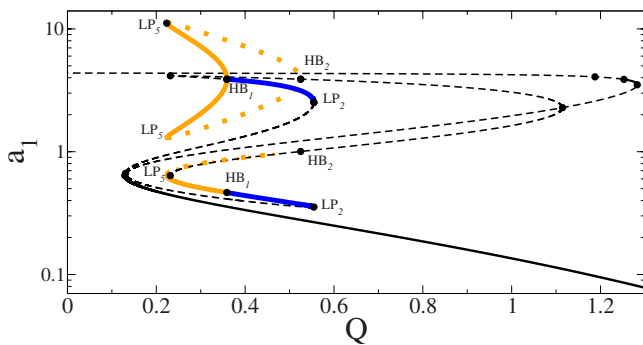


FIG. 4. (Color online) Bifurcation diagram versus coupling Q , with a focus on the IHLC and the IHSS. The stable IHSS is represented by a thick blue line, the stable IHLC with a thick orange line, and the unstable IHLC is represented with a dashed yellow line. Parameters are those of Fig. 2.

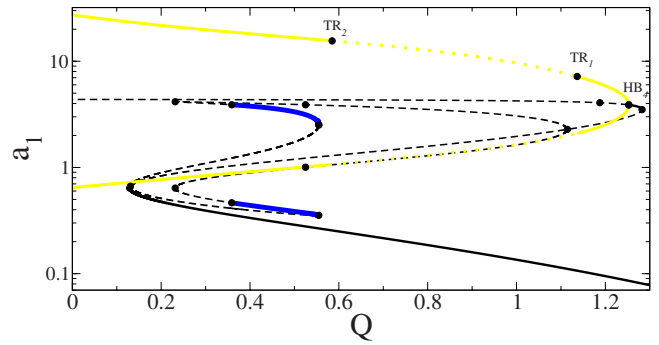


FIG. 5. (Color online) Bifurcation diagram versus coupling Q , focusing on the stable antiphase oscillations (thick yellow line). Parameters are those of Fig. 2.

so-called “oscillation death” (OD) regime. This regime arises at a critical coupling $Q_{crit} = 0.3588$ for the set of parameters used here, and is stable until LP_2 at $Q = 0.5548$. The IHSS solution coexists in the Q parameter space with the HSS (Fig. 3). For example, for $Q = 0.37$ there is a coexistence of nine steady-state solutions, three of them stable and six unstable.

The next step of the bifurcation analysis is to study the limit cycles that arise from the Hopf bifurcations found on the basic continuation curve. In particular, the Hopf bifurcation HB_1 gives rise to a branch of stable inhomogeneous periodic solutions, known in the literature as inhomogeneous limit cycle (IHLC) [23]. The manifestation of this regime is however different in different systems: For two identical diffusively coupled Brusselators, e.g., it is defined to be a periodic solution of the system of oscillators rotating around two spatially nonuniform centers [23,24]. For the model investigated here, the manifestation of the IHLC is somewhat different: The IHLC is characterized by a complex behavior, where one of the oscillators produces very small oscillations of the protein level, whereas the other one oscillates in the vicinity of the steady state with an amplitude just slightly smaller than that of an isolated oscillator [see Fig. 2(b)]. The IHLC is stable for values of Q between HB_1 and LP_5 (Fig. 4). In the case of the two-oscillator system considered here, each oscillator has the same probability to occupy and stay in the upper or lower state, due to the symmetry of the system. The initial conditions are the only factor determining the separation of the oscillators.

For coupling values smaller than a given critical value $Q_{crit} < 0.129$, the system is characterized by a self-oscillatory solution. For two coupled oscillators, this regime corresponds to antiphase oscillations. As shown on Fig. 5, this state belongs to a branch of periodic orbits originating at the Hopf bifurcation HB_4 . Figure 5 illustrates in detail the bifurcation structure of the antiphase dynamics when Q is being varied. Stable antiphase oscillations are observed between HB_4 ($Q = 1.253$) and TR_1 (torus bifurcation for $Q = 1.137$), and from $Q = 0$ until TR_2 ($Q = 0.5848$). As demonstrated, this solution loses its stability for $0.5848 < Q < 1.137$. Direct numerical simulations revealed the existence of complex behavior in the latter range of Q values, which we discuss in detail in Sec. V.

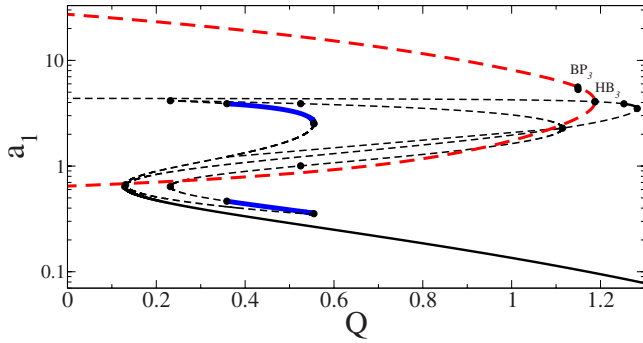


FIG. 6. (Color online) Bifurcation diagram versus the coupling Q where the periodic branch of the unstable synchronous oscillations (red dashed lines) is shown. Parameters as in Fig. 2.

In contrast to the case of positively coupled repressilators [5], where coupling was seen to provide coherence enhancement, investigations of the dynamical structure of the system with phase-repulsive coupling by means of direct calculations [13] did not reveal the presence of a stable in-phase regime (synchronous oscillations over the entire cell population). The present bifurcation analysis confirms this result: A branch of synchronous periodic oscillations is in fact seen to emanate from HB_3 , but it is unstable (Fig. 6). We have further confirmed that the in-phase regime is unstable for all values of α and Q studied, in contrast to the antiphase limit cycle oscillations, which arise even for small α values. The existence of this antiphase (or phase-shifted) solution is a clear manifestation of the phase repulsive character of the AI-mediated coupling, which enhances the phase difference between the oscillators in the model, until the maximal phase difference of $\frac{\pi}{2}$ is reached.

IV. COMPARISON BETWEEN BIFURCATION ANALYSIS AND DIRECT CALCULATIONS

To compare the bifurcation analysis with the results of direct calculations, we calculated 1000 time series for the system of two coupled repressilators with different random initial conditions for every parameter set, using an uniform distribution [25] in the range [0,220] for the mRNA and protein initial conditions and [0,1.2] for the AI initial condition. The 1000 random initial conditions cover the 14-dimensional phase space of the system (7 degrees of freedom per oscillator) densely enough such that one can detect stable coexisting attractors with a significant basin of attraction. The direct calculations described here represent a different approach from the bifurcation analysis, and are valid for large system sizes as well. Therefore, the combination of both methods sheds light on the dynamics of the repressilator model with repressive cell-to-cell communication. All the direct numerical simulations are performed in the same manner as in Ref. [13] for an ensemble of 100 repressilators.

Figure 7 (top) shows the stable-steady-state and limit-cycle branches as obtained from the bifurcation analysis, whereas the bottom plot represents the percentage of regimes as determined by the direct calculations described above. Both methods predict and confirm that for small coupling,

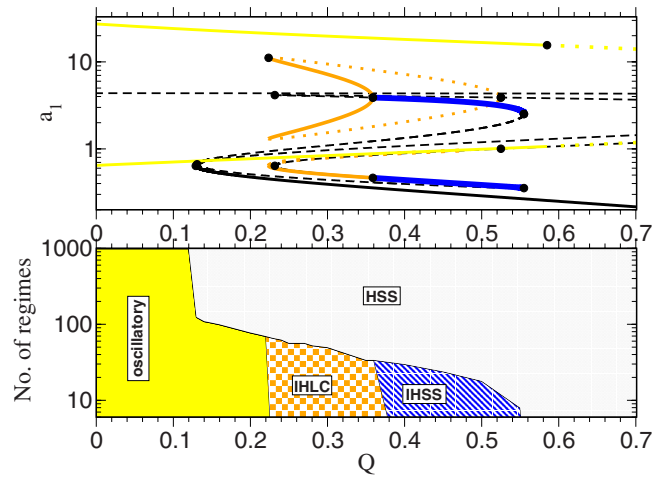


FIG. 7. (Color online) Comparison between the bifurcation analysis (top) and the direct calculation with random initial conditions (bottom). Note the logarithmic scale of both ordinates in the two plots. The oscillatory regime is represented by a yellow solid line (top) and a yellow area (bottom); the IHLC by solid orange lines (top) and a orange-white chess board pattern (bottom); the IHSS by solid blue lines (top) and a small blue striped area (bottom); and finally the HSS is illustrated by a solid black line (top) and a grey area (bottom). Parameters are those of Fig. 2.

$Q < 0.129$, antiphase self-oscillations are the only stable regime. For coupling value $Q=0.129$, the homogenous steady-state stabilizes through a limit point bifurcation (LP_1 in Fig. 3), and further coexists with an oscillatory solution. The direct calculations reveal the dominance of the single-fixed-point solution, which has a larger basin of attraction: At $Q=0.2$, for instance, only about 70 of the total 1000 random initial conditions result in the oscillatory state, while the other remaining 930 result in HSS. For $Q \in [0.2236, 0.3588]$, direct calculations show the existence of an inhomogenous limit cycle (orange white chessboard pattern in Fig. 7, bottom) that coincides with the region where a stable IHLC solution was found by the bifurcation analysis (solid orange line in Fig. 7, top). As previously discussed, the IHLC branch emerges via a Hopf bifurcation (HB_1 on Fig. 4), through which the IHSS loses stability as Q decreases. We see a very good coincidence of the stability ranges of the IHLC and the IHSS predicted by the bifurcation analysis and shown by the direct calculation. Both regimes have a small basin of attraction. Note however that in the region where the IHLC and IHSS exist, the bifurcation analysis predicts the coexistence of the antiphase oscillatory regime, which is nevertheless not observed in the direct simulations. This is due to the fact that the antiphase oscillations have a very small basin of attraction, which is difficult to reach from a set of initial conditions drawn randomly throughout the 14-dimensional phase space of the system.

V. CHAOS PROVOKED BY REPRESSIVE CELL-TO-CELL COMMUNICATION

The bifurcation analysis (Fig. 5) predicts unstable antiphase oscillations between the torus bifurcation points TR_2

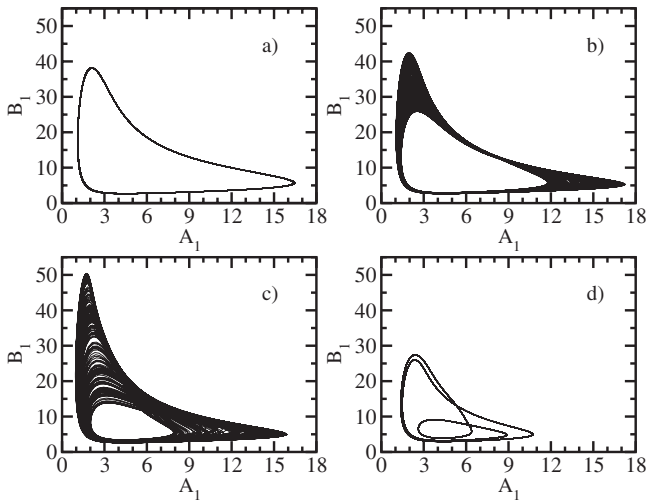


FIG. 8. Phase diagrams of the self-oscillations in the A_1 - B_1 plane for large coupling Q : (a) $Q=0.5$, (b) $Q=0.6$, (c) $Q=0.7$, and (d) $Q=0.96$. Other parameters are those in Fig. 2.

and TR_1 . We could not trace the solutions emerging from those bifurcations with XPPAUT, and proceeded the investigations with direct calculations. To that end, we performed simulations starting with small coupling Q and traced the self-oscillatory regime up to strong coupling. The resulting self-oscillations are stable and resistant to small perturbations in the initial conditions and to dynamical noise (mRNA dynamics was perturbed with additive white noise, corresponding results not presented here). Figure 8 shows phase plots for different values of Q . Figure 8(a) with $Q=0.5$, just before the torus bifurcation TR_2 , shows normal self-oscillations in the A_1 - B_1 phase plane. Figure 8(b) corresponds to a Q value just after the torus bifurcation, and shows the projection of the torus in the A_1 - B_1 phase plane. The phase plots of Figs. 8(c) and 8(d) also correspond to Q values between the two torus bifurcations TR_2 and TR_1 , but look very different. Specially, Fig. 8(c) may correspond to chaotic dynamics.

To reveal and classify the different self-oscillatory dynamics between the two torus bifurcations, we compute the maximal Lyapunov exponent of the system. To that end, we forward integrate a small perturbation of the trajectory, the random tangent vector, by the Jacobi matrix. The logarithm of the norm of the tangent vector is related to the maximal Lyapunov exponent [26] and we normalize it by the integration time. The result is shown in Fig. 9, together with a bifurcation diagram computed as a series of Poincaré sections, with the ordinate showing the value of the B_1 if the trajectory crosses $A_1=4.0$.

A torus bifurcation implies an increase of the dimensionality of the attractor. To confirm this fact we computed the correlation dimension D_2 of the system, which verifies that $C(\varepsilon) \sim \varepsilon_2^D$, where $C(\varepsilon)$ is the correlation sum and ε the size of the balls in which the phase-space is partitioned. The correlation sum measures the number of pairs of attractor points inside the ε ball [27]. We calculate the correlation sum and the correlation dimension with the TISEAN package [28], making use of the time series of all 14 variables, in such a

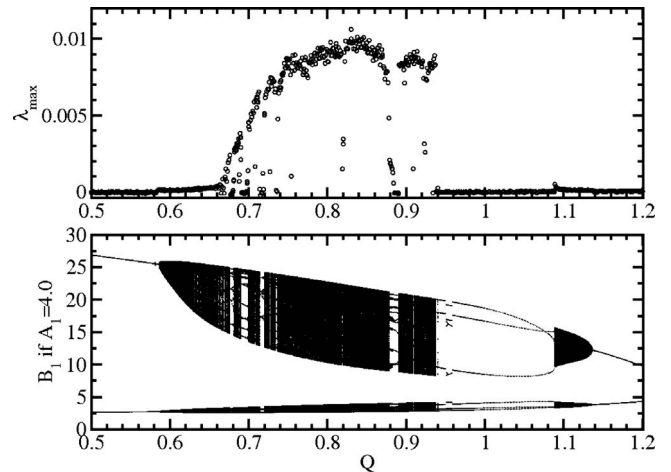


FIG. 9. Maximal Lyapunov exponent (top) and the corresponding bifurcation diagram (bottom) versus coupling Q . Parameters as in Fig. 2.

way that a phase-space embedding of the dynamics is not necessary. The resulting dimension of the stable self-oscillatory attractor is much smaller than the dimension of the system. Figure 10 shows the correlation sum versus ε for diverse values of the coupling strength Q . In Fig. 10, the results are separated in two groups, for $0 < Q < 1$ [Fig. 10(a)] and $Q \geq 1$ [Fig. 10(b)] for clarity. The correlation dimension corresponds to the slope of the resulting curves in these double logarithmic plots.

Limit-cycle oscillations appear below the torus bifurcation $Q < TR_2 \approx 0.587$. The slope of the correlation sum for $Q=0.5$ [Fig. 10(a)], and hence the correlation dimension, is $D_2=1$ as one expects from limit cycle oscillations. The limit

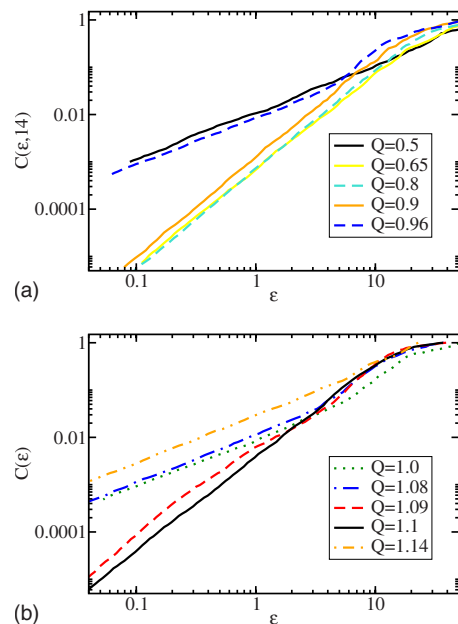


FIG. 10. (Color online) Correlation sum $C(\varepsilon)$ for (a) the biologically relevant range $Q \in [0, 1]$, and (b) Q outside of the biologically relevant range (only for theoretical completeness and justification of Fig. 9).

cycle is confirmed by the bifurcation diagram (Fig. 9, bottom) and by the value of the maximal Lyapunov exponent ($\lambda_{\max} \approx 0$, Fig. 9, top).

At $Q \approx 0.587$ the regular oscillations disappear and the trajectory fills up a growing dense space. The onset coincides with the first torus bifurcation TR_2 (secondary Hopf bifurcation) in the bifurcation analysis (Fig. 5). The maximal Lyapunov exponent remains unaffected by the torus bifurcation at $\lambda_{\max} \approx 0$. The correlation dimension increases up to $D_2=2$, because the slope of the correlation sum for $Q = 0.65$ [Fig. 10(a)] is 2 times that for $Q=0.5$.

At $Q \approx 0.67$ the torus attractor becomes unstable and λ_{\max} increases significantly above zero, marking the onset of chaotic behavior. The chaotic regime ranges up to $Q \approx 0.937$ and is interrupted by periodic windows at some intermediate ranges of Q . For instance, for $Q \in [0.879, 0.89]$ the maximal Lyapunov exponent λ_{\max} drops down up to zero and the bifurcation diagram shows periodic windows in the otherwise densely occupied phase plane. Outside those windows the correlation dimension is slightly above two, and must in fact be fractal due to the positive value of the maximal Lyapunov exponent. As an example, we plot the correlation sum for the coupling values $Q=0.8$ and $Q=0.9$ [Fig. 10(a)] and one can see that the slopes are slightly steeper than the one of $Q = 0.65$. The chaotic dynamics results in a fractal structure of the attractor with a dimension slightly above two. The Kaplan-Yorke formula relates the Kaplan-Yorke dimension with the set of Lyapunov exponents and predicts that a weak unstable limit cycle with a small positive maximal Lyapunov exponent results in only a bit larger noninteger dimension [29].

The chaotic region ends abruptly at $Q \approx 0.937$, at which point λ_{\max} declines to zero and the bifurcation diagram reveals a relatively simple structure. A phase plot at $Q=0.96$ can be seen in Fig. 8(d). The limit cycle is confirmed by the correlation dimension being $D_2=1$, as shown for $Q=0.96$, $Q=1.0$, and $Q=1.08$ [Figs. 10(a) and 10(b)]. Values of Q beyond 1 are outside the biological relevant range, but are helpful to understand the dynamics in the region between TR_2 and TR_1 , and to show the coincidence of the bifurcation analysis and the direct calculations.

The interval $Q \in [1.089, 1.137]$ is characterized by torus oscillations without chaotic dynamics. The maximal Lyapunov exponent remains at $\lambda_{\max} \approx 0$ (Fig. 9) and the correlation dimension is $D_2=2$, as one can see from the slopes of the correlation sum for $Q=1.09$ and $Q=1.1$ [Fig. 10(b)]. The bifurcation at $Q \approx 1.089$ could be a tangent bifurcation.

The torus bifurcation at $Q \approx 1.137$ changes the torus to a limit cycle and coincides with the torus bifurcation TR_1 of the bifurcation analysis (Fig. 5). As one expects for limit-cycle oscillations $\lambda_{\max} \approx 0$ and $D_2=1$ [see the slope of the correlation sum in Fig. 10(b)].

We note that both the self-oscillatory (as discussed in the preceding section) and the chaotic regimes have a rather small basin of attraction, which makes it very difficult to reach those regimes from a random sampling of initial conditions in phase space, as done in Fig. 7. Thus, it is not clear whether chaotic dynamics would be observed in an experimental implementation of our model. However, following the spirit of the results that have been presented in this sec-

tion, one could envisage an experimental protocol in which a cell population starts from the self-oscillatory regime with small Q , i.e. small cell density, and smoothly increases its density due to replication. In that case, one could expect the system to end in a self-oscillatory regime at high cell density Q , and possibly in a chaotic regime. That experiment protocol would be comparable with the numerical method that we have used in this section. Therefore, even though the numerical results presented here are rather speculative in the context of real genetic circuits, they should draw attention to possible alternative sources of uncertainty in biological systems.

VI. SUMMARY AND OUTLOOK

In this paper, we present investigations of two modified repressilators, coupled by the fast diffusion of the AI across the cell membranes. We show that, after the modifications we have introduced in the model, the diffusion of the AI governed through the slow time scale of the system provides a phase-repulsive coupling, which, in turn, results in a rich and very unusual multistability of the system. We demonstrate the coexistence of stable homogenous, stable inhomogeneous steady states, and stable oscillating regimes in a broad region of parameter space.

The model considered and the coupling we have introduced [Eqs. (7)–(9)] have specific properties compared to other coupled oscillators [30,31]. Typically, coupling in population is realized via special channels (e.g., gap junctions in Astrocytes [32]), thus the coupling substance is not diluted in the medium. This means that a coupling term similar to the one governed by η in Eq. (7) determines the coupling strength in standard situations. In our case, on the other hand, the parameter Q regulates how much AI is returned to cells from the medium. For small Q the two oscillators show only a stable antiphase limit cycle. This predicts the dominance of three-cluster decompositions in multicellular ensembles [13]. For larger Q auto-oscillating regimes coexist with HSS and IHSS, as well as with IHLC. The probability of a specific regime realization depends on the initial condition, which are in turn the results of system evolution if we are dealing with growing population and/or external perturbations.

The above-discussed repressilator with repressive cell-to-cell communication shows chaotic dynamics in a biologically reasonable parameter range. Usually, random fluctuations in protein production are assumed to be caused by noise, of either intrinsic or extrinsic origin [33]. Our results suggest that chaotic dynamics might be an additional source of uncertainty in gene expression, which can exist in parallel to noise. The weak chaotic behavior observed is evoked by cell-to-cell communication, and could not be found in the uncoupled repressilator model. The chaotic dynamics and the torus oscillations coexist with HSS (Fig. 7) and each dynamical regime is stable and robust to small noise. Sufficient noise could evoke rare jumps from one stable regime to another one, followed by long periods without dynamical changes. In that sense, the paradigmatic repressilator with the

many multistable states could be an example of the importance of rare events in biological systems with deep behavioral changes, including chaos. Biological systems typically exhibit diversity, and considering identical oscillators is a strong simplification. Therefore, we tested the stability of the dynamical regimes by applying independent additive noise to the mRNA dynamics and introduced a small individual difference in the parameter α amongst the oscillators. Preliminary results in nonidentical repressilators (not shown) reveal the robustness to perturbation of the four regimes IHLC, IHSS, HSS, and antiphase self-oscillations. Diversity is of special interest and a detailed investigation of that effect in ensembles of coupled repressilators is currently in progress.

ACKNOWLEDGMENTS

E.U. acknowledges financial support from the Alexander von Humboldt Foundation, A.K. and J.K. acknowledge the GoFORSYS project funded by the Federal Ministry of Education and Research, Grant No. 0313924, J.K. acknowledges the EU through Network of Excellence BioSim, Contract No. LSHB-CT-2004-005137, E.V. acknowledges support from the Program “Radiofizika” Russian Academy and RFBR Grant No. RFBR 08-02-00682, and J.G.O. acknowledges support from the Ministerio de Educación y Ciencia (Spain) (project ORDEN and I3 program). This work has also been supported by the European Commission (project GABA, FP6-NEST Contract No. 043309).

-
- [1] T. S. Gardner, C. R. Cantor, and J. J. Collins, *Nature (London)* **403**, 339 (2000).
- [2] M. Elowitz and S. Leibler, *Nature (London)* **403**, 335 (2000).
- [3] A. Kuznetsov, M. Kærn, and N. Kopell, *SIAM J. Appl. Math.* **65**, 392 (2004).
- [4] R. Weiss, S. Basu, S. Hooshangi, A. Kalmbach, D. Karig, R. Mehreja, and I. Netravali, *Natural Comput.* **2**, 47 (2003).
- [5] J. García-Ojalvo, M. B. Elowitz, and S. H. Strogatz, *Proc. Natl. Acad. Sci. U.S.A.* **101**, 10955 (2004).
- [6] E. I. Volkov and M. N. Stolyarov, *Phys. Lett. A* **159**, 61 (1991).
- [7] S. K. Han, C. Kurrer, and Y. Kuramoto, *Phys. Rev. Lett.* **75**, 3190 (1995).
- [8] G. Balázsi, A. Cornell-Bell, A. B. Neiman, and F. Moss, *Phys. Rev. E* **64**, 041912 (2001).
- [9] H. Meinhardt, *Models of Biological Pattern Formation* (Academic, New York, 1982).
- [10] R. Laje and G. B. Mindlin, *Phys. Rev. Lett.* **89**, 288102 (2002).
- [11] L. Glass and M. C. Mackey, *From Clocks to Chaos: The Rhythms of Life* (Princeton University Press, Princeton, NJ, 1988).
- [12] A. Koseska, E. Volkov, A. Zaikin, and J. Kurths, *Phys. Rev. E* **75**, 031916 (2007).
- [13] E. Ullner, A. Zaikin, E. I. Volkov, and J. García-Ojalvo, *Phys. Rev. Lett.* **99**, 148103 (2007).
- [14] J. Hasty, F. Isaacs, M. Dolnik, D. McMillen, and J. J. Collins, *Chaos* **11**, 207 (2001).
- [15] D. McMillen, N. Kopell, J. Hasty, and J. J. Collins, *Proc. Natl. Acad. Sci. U.S.A.* **99**, 679 (2002).
- [16] L. You, R. S. Cox III, R. Weiss, and F. H. Arnold, *Nature (London)* **428**, 868 (2004).
- [17] H. R. Horton, L. A. Moran, R. S. Ochs, J. D. Rawn, and K. G. Scrimgeour, *Principles of Biochemistry*, 3rd ed. (Prentice Hall, New York, 2002).
- [18] B. Ermentrout, *Simulating, analyzing and animating dynamical systems: A guide to XPPAUT for researchers and students (software, environment and tools)*, 1st ed. SIAM, 2002.
- [19] K. Bar-Eli, *Physica D* **14**, 242 (1985).
- [20] M. Dolnik and M. Marek, *J. Phys. Chem.* **92**, 2452 (1988).
- [21] M. F. Crowley and I. R. Epstein, *J. Phys. Chem.* **93**, 2496 (1989).
- [22] K. Tsaneva-Atanasova, C. L. Zimlik, R. Bertram, and A. Sherman, *Biophys. J.* **90**, 3434 (2006).
- [23] J. Tyson and S. Kauffman, *J. Math. Biol.* **1**, 289 (1975).
- [24] E. I. Volkov and V. A. Romanov, *Phys. Scr.* **51**, 19 (1995).
- [25] W. H. Press, S. A. Teukolsky, and W. T. Vetterling, *Numerical Recipes in C: The Art of Scientific Computing*, 2nd ed. (Cambridge University Press, Cambridge, 1993).
- [26] J. P. Eckmann and D. Ruelle, *Rev. Mod. Phys.* **57**, 617 (1985).
- [27] H. Kantz and T. Schreiber, *Nonlinear Time Series Analysis*, 2nd ed. (Cambridge University Press, Cambridge, 2004).
- [28] R. Hegger, H. Kantz, and T. Schreiber, *Chaos* **9**, 413 (1999).
- [29] P. Grassberger and I. Procaccia, *Physica D* **9**, 189 (1983).
- [30] Y. Zhai, I. Z. Kiss, and J. L. Hudson, *Phys. Rev. E* **69**, 026208 (2004).
- [31] G. B. Ermentrout and N. Kopell, *SIAM J. Appl. Math.* **54**, 478 (1994).
- [32] G. Ullah, P. Jung, and A. H. Cornell-Bell, *Cell Calcium* **39**, 197 (2006).
- [33] M. Elowitz, A. Levine, E. Siggia, and P. Swain, *Science* **297**, 1183 (2002).